Deep Learning-Based Segmentation of Early-Stage In-Bag Rice Root for Its Architecture Analysis

Kai Zhu[1], Liang Gong[1*], Chenghui Lin[1], Tao Wang[1], Ke Lin[1], Da Jing Gu, Chengliang Liu[1*], Third Author[1,2]

[1]School of Mechanical Engineering, Shanghai Jiao Tong University, Shanghai 200240, China

[2]ParisTech Elite Institute of Technology, Shanghai Jiao Tong University, Shanghai 200240, China

*** Correspondence:**

Chengliang Liu
profchlliu@163.com

Liang Gong
gongliang_mi@sjtu.edu.cn

Keywords: Plant root$_1$, Image processing$_2$, Image segmentation$_3$, Deep-learning$_4$, Convolutional neural network$_5$.

Abstract

The root architecture parameters are important to the study of plant growth state and the segmentation of plant roots is the key to the measurement of these parameters. Most existing methods use the threshold calculated by different algorithms to segment the roots in a grayscale image, which requires a low noise background. We designed an automatic equipment to record the roots images of rice seedlings planted in transparent bags. Those root images contain strong noise and it makes existing methods invalid in our circumstances. In order to solve the segmentation problem of rice roots under strong noise, we proposed a convolutional neural network based on U-Net and SE-ResNet. The root images were preprocessed and cropped into small patches to fit CNN input requirements. Experiments have showed that our method performs effectively in pixel-level segmentation of rice seedling roots that contain tiny lateral roots. Our method achieves an intersection over union (IoU) of 87.4%. This method provides a new approach to automatic and fast pixel-level root segmentation, which is of great importance for the attribute analysis of root morphology.

1 Introduction

The root system is the key organ of a plant to extract nutrients and water from the soil (Aroca, Porcel, & Ruiz-Lozano, 2012). It contains the growth information and reveals the health state of the plant. The research of plant root systems is very significant in biological field (Zobel, Kinraide, Baligar, & Soil, 2007), as it is an important way to improve grain production. Root morphological attributes are useful while evaluating the tolerance of plants to the fluctuation of growth conditions (Sekulska-Nalewajko & Goclawski, 2009). Determining the parameters of root morphological characteristics and analyzing root architecture are the crucial steps of root morphological attributes analysis.

However, the root features are hard to extract manually. Fortunately, some auto-analysis methods of digital images have made this procedure more efficient (Andr és et al., 2008). The root system segmentation is the foundation of most root morphological attributes analysis. Generally, the segmentation of root objects means recognizing the root from the background in images (Strack,

2001). A Large number of segmentation methods have been proposed. (Y. Chen & Zhou, 2010) used the Otsu method to segment the root images after median filtering, which is an image segmentation algorithm based on dynamic threshold. (Gocławski, Sekulska-Nalewajko, Gajewska, & Wielanek, 2009) proposed a new method based on the color features of the wheat seedlings' roots. The image was transformed into HCI from RGB color space firstly. Then threshold of component images were selected. The transformation of color space is quite useful. (Sekulska-Nalewajko & Goclawski, 2009) implemented the segmentation after the image had been transformed into HSI color space.

Although various methods have been used for root segmentation, almost all of them are limited to a certain kind of root images under specific circumstances (Gocławski et al., 2009). Also, those methods preferred simplex roots and oversimplified background to ensure the high contrast between the root and background, which is the critical factor for the segmentation methods based on threshold. Generally, if the root maintains its primitive condition without being washed or stained, the collected images are very likely to have a low contrast so that the methods based on threshold will be invalid. Meanwhile, the rice root system is composed of several tissues and there are different root types, which form a complex structure (Rebouillat et al., 2009). That increases the segmentation difficulty of the existing methods. The root images used in this paper are from the rice seedlings that were planted in the transparent bags. Those images contain the reflective light and water drops, which interfere the segmentation. As deep learning has achieved unparalleled results in computer vision tasks, particularly the convolutional neural networks (CNN) inspired by the organization of the visual field (Hubel & Wiesel, 1968), the accuracy of object detection and semantic segmentation has been remarkably improved. Apparently, CNN can be used successfully in the life sciences (Zhou & Troyanskaya, 2015), though the status might be more complex. In fact, the deep learning has already been used for plant root analysis. (Pound et al., 2017) proposed a CNN model to classify the sliding window over the root images. The wheat root tips are identified and localized after the whole root image is scanned by the sliding window. (Ke et al.) used a CNN model for cucumber powdery mildew recognition. (Yao, Zhang, & Xu, 2016) applied a CNN network for retinal blood vessel segmentation with 23*23 image patches extracted from blood vessel images.

To solve the difficulties in root segmentation brought by the complex structure of rice root and the strong noise in the images, a deep learning model of semantic segmentation is proposed. The proposed CNN model uses the processed root images as the input and the mask images as the output. The results show that our method performed quite well on rice root images with strong noise.

2 MATERIALS AND MOTHODS

2.1 Data Collection

In order to acquire the root image while keeping the roots' primitive shape, the rice seedlings should not be moved during the processes. Some experiments use the MRI or X-ray to obtain roots under the soil, although the equipment is quite expensive. Another solution is planting the rice seedlings in the transparent medium to facilitate root image acquisition. But there has been little research about that, the result of (Tracy, Black, Roberts, & Mooney, 2010) shows that the properties of medium had a significant effect on root weight and root configuration. (Iyer-Pascuzzi et al., 2010) grew the rice seedlings in the Gelzan CM agar to investigate the root traits which can distinguish rice genotypes. This method is quite outstanding for obtaining root images except the demand for the expensive equipment. However, the quantity and diversity of the image samples are the factors influencing the capability of a CNN model (Barbedo, 2018). In this paper, we use transparent bags filled with nutrient solution to cultivate the rice seedlings and the experiments have shown that the root can

cling to the capillary paper in these transparent bags. Figure 1 shows the captured root image of the early-stage in-bag rice seedlings with the roots longer than 10 cm.

A multi-angle camera layout is adopted to improve the efficiency of image capturing and a light source is installed on the side along with a bottom light to minimize the reflection. To avoid the interference of ambient light, the imaging equipment is mounted in a darkroom. As shown in Figure 2, four cameras are installed in different angles to capture four root images each time. The shell of the darkroom is made of aluminum-profile frame wrapped with metal skin to cut off the ambient light. There is a conveyor belt and a window for transporting rice seedlings into this device, and the window will be closed when the cameras start working. This procedure is controlled by a PLC that receives the signals generated by the sensors mounted on the equipment. We used the CCD industrial cameras with a resolution of 4608×3288 pixels, which will ensure the detection of the lateral roots.

2.2 Image Process

As shown in Figure 1, the original images contain part of the background and it is uncorrelated data. The rice roots stretch like the thin strip, which is similar to the periphery of the background in morphology. This will be difficult for the network to achieve precise segmentation if the original images are directly used to train the CNN. We trimmed the useless part of pictures off and separated the root system of different seedlings as shown in Figure 3(a). The mask images of the root system were made manually with the help of Photoshop (Adobe Inc., USA). Usually, the size of a root image with single seedling is larger than 500×2000 pixels, which is too large to be used as the input data of a CNN. However, the down-sampling process brings the loss of information of small scale. Particularly, in this experiment, the lateral root is so tiny that it just occupies about 3 pixels in width. The lateral roots would be lost after the down-sampling. To solve this problem, we used a sliding window with the size of 100×100 pixels to scan root images and each patch of scanning results together with its mask image is considered as a sample for the CNN training.

Figure 3(b) is the mask of a root image and it is obvious that the white pixels standing for roots just take up a very small proportion in the image. Generally, the severe class imbalance will cause several problems (Lin et al., 2017). For example, the training will be inefficient. The model will degenerate because it tends to predict pixels to be negative as most pixels of the training images are negative. To avoid this condition, we set a threshold α and mark the proportion of white pixel in the sliding window as γ. The stride of the sliding window is set as half of the window size if γ is bigger than α, otherwise the stride is set as the size of the window. Specially, if $\gamma = 0$, the stride is set bigger than the size of sliding window. These tricks can help to reduce the imbalance of pixel class by increasing the proportion of root pixels. Figure 3(c) shows the stride of sliding window with different γ.

2.3 CNN Network Design

Many CNNs have achieved pixel-level segmentation to deal with the segmentation task for detailed patterns. The skip-architecture was proposed to accomplish detailed segmentation (Long, Shelhamer, & Darrell, 2015). It concatenated high-level features in encoding layers and appearance features in decoding layers, which is proved to be effective on natural images (Hao, Yang, Liu, Mo, & Guo, 2017). The U-Net is a kind of CNN using the skip-architecture and has achieved outstanding performance on biomedical image segmentation of different applications (Ronneberger, Fischer, & Brox, 2015). After the down-sampling and up-sampling process, output images have the same size with input images and the roots are segmented. These architectures help the U-Net combine the information of different scales and enhance the precision of edges. As the characteristic of root images are quite similar to the biomedical images, we chose the U-Net as the backbone of our CNN

model. In addition, the U-Net performs well on small dataset, which is useful as the obtention and annotation of root images are difficult.

To improve the performance of our model, we embedded the ResNet module and squeeze-and-excitation (SE) block into our model. The ResNet module is proposed to train a deeper neural network (He, Zhang, Ren, & Sun, 2016), as the trouble of gradients vanishing/exploding is a big obstacle when training a deeper neural networks. The SE-block is trained to recalibrate the response of different channel-wise features and find the interdependencies between channels (Hu, Shen, Albanie, Sun, & Wu, 2017). More detailed, the SE-block combined with the ResNet module called SE-ResNet module, was used to replace the convolution layer in U-Net. Figure 4 shows the structure of ResNet module and SE-ResNet module. The actual structure of SE-ResNet module used in this paper is on the right side of Figure 4. The residual module is consisted of one ReLU layer and two convolution layers. It has been demonstrated that SE-ResNet can significantly improve the performance of CNN with minimal extra computational cost. Meanwhile, the increase of weights can be ignored when compared to the total weights of the CNN. That means the embedding of SE-block will not cause the problem of overfitting.

The structure of our CNN model called SE-ResUnet is instructed in Figure 5. The architecture of our model includes a encoding path and a decoding path. Each colored rectangle stands for a module of neural network and has been explained in the figure. The pair of number under the rectangle indicates the size of output data in this layer and the number upon the rectangle indicates the channel quantity of this layer. The encoding path contains 5 neural network blocks. Except the input layer and the max-pooling layer, each block consists of a convolutional layer with a filter size of 3×3 pixels and two SE-ResNet modules mentioned before. Correspondingly, the decoding path has a deconvolutional layer concatenated with the copy of previous layer output, a convolutional layer with a filter size of 3×3 pixels and two SE-ResNet modules. The patches were upsampled to 128×128 before training. During the encoding, the number of feature map increases from 1 to 256 and the size of image decreases from 128×128 to 8×8 pixels. During the decoding, the number of feature map decreases from 256 to 1 and the size of image increases from 8×8 to 128×128 pixels. To avoid overfitting, we add a dropout layer after each max-pooling layer and deconvolutional layer (Srivastava, Hinton, Krizhevsky, Sutskever, & Salakhutdinov, 2014). In summary, our model is quite different with the original U-Net in content, although they are similar in form. The difference guarantees a good result of root segmentation.

The output layer of our model is a convolutional layer with a filter size of 1×1 and one channel. The output layer is activated by the sigmoid function. The value of each pixel represents the probability. Normally, the pixel is marked as root if its value is bigger than 0.5. Particularly, we use a threshold to determine whether the pixel belongs root or not. The threshold is chosen to help the metric function perform better on the validation data. The metric function is used to evaluate the result of segmentation.

2.4 Training and Optimization

As illustrated above, we used the sliding window to obtain more than 7000 patches from 30 root system images with large resolution as the dataset for training and validation. To improve the generalization ability of the model, we applied some tricks of data augmentation such as flip. Meanwhile, the annotation images were processed in the same way. In order to ensure the diversity of test data split from the dataset, we divided the images into 10 grades standing for the proportion of root region. In each grade, 10% of the patches were split as the validation set for parameter tuning

and the left was split as train set. Another 4 root system images were cut into patches as test set without being balanced or augmented for evaluate the final model performance.

Here we used the binary cross-entropy loss(cost) function (H. Chen, Li, Chen, & Tang, 2016) as shown in Equation 1. y_i stands for the ground truth of the pixel and p_i denotes the prediction value calculated by the model. The optimization algorithm we chose to minimize the loss function is the adaptive moment estimator (Adam) (Kingma & Ba, 2014). In Adam, the first and second moments of gradients are used for updating and correcting the current learning rate (Hao et al., 2017). During the training process, the parameters of Adam optimizer were set with initial learning rate = 0.01 and the maximum number of epochs = 75. The other parameters were kept as their default value. The learning rate would decay with the factor of 0.5 if there is no improvement in more than 5 epochs and the minimal learning rate was set as 0. The batch size was 32 and the input images were converted to grayscale with value between 0 and 1.

$$\boldsymbol{Loss} = \sum_{\boldsymbol{i=1}}^{\boldsymbol{m}} -(\boldsymbol{y_i}\, \boldsymbol{log}(\boldsymbol{p_i}) + (\boldsymbol{1} - \boldsymbol{y_i})\, \boldsymbol{log}(\boldsymbol{1} - \boldsymbol{p_i})) \quad (1)$$

Our model was implemented with Keras, which is a high-level neural network deep learning API written in Python with TensorFlow, CNTK, or Theano backend. We trained our model on a GPU server with the Ubuntu 16.04 operating system and it costs 4 hours to finish the training with one NVIDIA GeForce GTX 1080 GPU.

2.5 Performance Evaluation

Here we use the intersection over union (Long et al., 2015) and dice accuracy (Milletari, Navab, & Ahmadi, 2016) as the metrics. The pixel Hausdorff Distance is also considered. The intersection over union(IoU) can evaluate the model performance effectively and eliminate the interference of overmuch negative sample. The dice accuracy(DSC) indicates the overlap measurement between the ground truth root regions and the segmentation results (prediction) of our model.

Those metrics are calculated by Equation 2, 3,4, where the *TP*, *FP* and *FN* denote the true positive(the area which is both predicted and annotated as root area), false positive(the area which is predicted as root area but annotated as background) and false negative(the area which is predicted as background but annotated as root area) measurements. In Equation 2, $\boldsymbol{X} = \{\boldsymbol{x_1}, \boldsymbol{x_2}, \boldsymbol{x_3} \ldots\}, \boldsymbol{Y} = \{\boldsymbol{y_1}, \boldsymbol{y_2}, \boldsymbol{y_3} \ldots\}$ stands for two point sets (the root pixels).We extracted 10% of the total dataset to calculate the metrics mentioned above.

$$\begin{cases} \boldsymbol{d_H} = \boldsymbol{max}\{\boldsymbol{h}(\boldsymbol{X}, \boldsymbol{Y}), \boldsymbol{h}(\boldsymbol{Y}, \boldsymbol{X})\} \\ \boldsymbol{h}(\boldsymbol{X}, \boldsymbol{Y}) = \boldsymbol{max}_{\boldsymbol{x} \in \boldsymbol{X}}\{\boldsymbol{min}_{\boldsymbol{y} \in \boldsymbol{Y}}\{\|\boldsymbol{x} - \boldsymbol{y}\|\}\} \end{cases} \quad (2)$$

$$\boldsymbol{IoU} = \frac{\boldsymbol{TP}}{\boldsymbol{FP+TP+FN}} \quad (3)$$

$$\boldsymbol{DSC} = \frac{\boldsymbol{2TP}}{\boldsymbol{FP+2TP+FN}} \quad (4)$$

3 Result

The proposed CNN was employed on our root dataset and the result shows that our model has achieved excellent performance on root segmentation task. We achieve 87.4% on IoU. Those metrics demonstrated that our model had accomplished a favorable performance in root segmentation task for different evaluation criteria. Our CNN model was developed with Keras using a Tensorflow backend. We trained 75 epochs on one NVIDIA GeForce GTX 1080 GPU.

Figure 6 shows the loss value and IoU accuracy of the proposed CNN model used on the root segmentation task during the training process. The loss reduced and tended to be gentle on training dataset, while the IoU increased and tended to be gentle. As shown in Figure 6, the loss and IoU tendency of validation dataset is the same with train set, indicating the model was well trained and had no overfitting.

We used the trained model to implement the segmentation on a typical root system image and the result is shown in Figure 7. The root system was segmented accurately and both the taproot and lateral root were separated with the background correctly as shown in Figure 7,8. In Figure 7(a), the noise similar to lateral root was removed, demonstrating that our proposed method was robust. As the CNN requires images with size of 128 pixels, we trimmed the whole test root image into patches to fit the CNN input. Each patch was segmented and saved in order, so that they can be stitched into a complete root system image.

4 Discussion

4.1 Comparison

To illustrate the performance of the proposed model, we reproduced the experiment using the method proposed by (Y. Chen & Zhou, 2010) as a comparison, where the Otsu method was used to segment the root after median filtering. Meanwhile, it is necessary to compare the proposed method with U-Net and investigate the effect of incorporating SE-ResNet.

Figure 8 shows the convergence process of loss and IoU for U-Net. Compared with the convergence process of our model in Figure 6, the IoU convergence speed is slow than proposed model and final IoU value is also smaller. The experiment result strongly proved the effectiveness of our model.

Table 1 shows the values of Hausdorff distance, DSC and IoU for the previously mentioned methods, when they are applied to the test set. Obviously, the result of deep learning methods are much better than Otsu method. It is worth noting that metrics of deep learning methods on test set are better than it on either train set or validation set. This phenomenon is understandable as the test set was obtained without being balanced. Our method excels than U-net at all three metrics, which shows that our method is more effective.

As shown in Figure 9(b), the taproot is segmented correctly and part of lateral roots is distinguished. The continuity of the final image is not influenced by using sub-images as the input of our CNN model, since the sub-images and origin images are similar in structural features. However, due to the low contrast of lateral root and background, most pixels of lateral roots are classed as background. As shown in Figure 9(c)(d), the deep learning method performs much better than the Otsu method. Most pixels of lateral roots are classed correctly. Meticulously, our method performs better in details, especially the end of lateral roots.

4.2 Limitations

Although many methods have been proposed to solve the problem of root segmentation, they are usually implemented in specific circumstances, where simple root and low noise background are demanded. These methods usually segment the root by determining a threshold, which decides the result of segmentation. Meanwhile, some processes have to be implemented to enhance the contrast. However, the materials used here contain much noise and the gray value distribution of lateral roots overlaps with the background, making those methods invalid. Based on the CNN's strong ability of feature extraction, our method can segment the roots successfully.

Unfortunately, there are some limitations in our method. Firstly, as shown in Figure 10, there are some mistakes in image annotation. The rice roots are so complex that we can not annotate every lateral root correctly and the slender morphological character of roots makes it hard to divide the boundary of root from background. Generally, the quality of image annotation determine the performance of CNN. As shown in Figure 10, not all lateral roots are segmented. These problems are caused by the errors of image annotation. Figure 11 shows the worst result, the lateral roots are too many to be segmented correctly.

To decrease the difficulty of making image annotation, image enhancement might be a choice to help improve segmenting the root correctly, for which it would increase the contrast between the root and background. (Koller, Gerig, Szekely, & Dettwiler, 1995) proposed a multiscale based image enhancement method to segment vascular image. Equally, applying these methods to the root images may help improve the performance of CNN model.

4.3 Conclusion

In this paper, we proposed a deep learning-based method to solve the problem of root segmentation. An automatic equipment was designed to acquire the images of rice roots cultivated in transparent bags. After the preprocessing, the root images were segmented by our CNN model.

Our SE-ResUnet model can segment the root images effectively. We achieved 87.4% on IoU. It is of great improvement when compared to the Otsu method. Our method achieved excellent performance on root segmentation, especially on the lateral root segmentation and noise elimination. The experiments show that our method can be used to realize the automatic root segmentation and it is important for the study of phenotypic parameters.

Conflict of Interest

The authors declare that the research was conducted in the absence of any commercial or financial relationships that could be construed as a potential conflict of interest.

Author Contributions

L.G., K.Z. conducted mathematical modeling and article writing. D.G. and T.W. helped building the data collection equipment. K.L. and C.L. conducted the experimental verification.

Funding

The research was funded by the Royal Society, CHL\R1\180496 and by the Shanghai Municipal Agricultural Commission, 2019-2-2.

Acknowledgments

The useful help and advice given by Linlizi Wu in sample collection and equipment design are gratefully acknowledged.

Reference

Andrés, C. K., Nagel, K. A., Klaus, P., Ulrich, S., Achim, W., & Hanno, S. J. N. P. (2008). Spatio-temporal quantification of differential growth processes in root growth zones based on a novel combination of image sequence processing and refined concepts describing curvature production. *177*(3), 811-821.

Aroca, R., Porcel, R., & Ruiz-Lozano, J. M. (2012). Regulation of root water uptake under abiotic stress conditions. *J Exp Bot, 63*(1), 43-57. Retrieved from https://www.ncbi.nlm.nih.gov/pubmed/21914658. doi:10.1093/jxb/err266

Barbedo, J. G. A. J. B. E. (2018). Factors influencing the use of deep learning for plant disease recognition. *172*, 84-91.

Chen, H., Li, Y., Chen, C. L., & Tang, X. (2016). *Learning Deep Representation for Imbalanced Classification.* Paper presented at the Computer Vision & Pattern Recognition.

Chen, Y., & Zhou, X. (2010). *Plant root image processing and analysis based on 2D scanner.* Paper presented at the IEEE Fifth International Conference on Bio-Inspired Computing: Theories and Applications.

Gocławski, J., Sekulska-Nalewajko, J., Gajewska, E., & Wielanek, M. (2009). An automatic segmentation method for scanned images of wheat root systems with dark discolourations. *International Journal of Applied Mathematics and Computer Science, 19*(4), 679-689. doi:10.2478/v10006-009-0055-x

Hao, D., Yang, G., Liu, F., Mo, Y., & Guo, Y. (2017). Automatic Brain Tumor Detection and Segmentation Using U-Net Based Fully Convolutional Networks.

He, K. M., Zhang, X. Y., Ren, S. Q., & Sun, J. (2016). Deep Residual Learning for Image Recognition. *2016 Ieee Conference on Computer Vision and Pattern Recognition (Cvpr)*, 770-778. Retrieved from <Go to ISI>://WOS:000400012300083. doi:10.1109/Cvpr.2016.90

Hu, J., Shen, L., Albanie, S., Sun, G., & Wu, E. (2017). Squeeze-and-Excitation Networks.

Hubel, D. H., & Wiesel, T. N. (1968). Receptive fields and functional architecture of monkey striate cortex. *J Physiol, 195*(1), 215-243. Retrieved from https://www.ncbi.nlm.nih.gov/pubmed/4966457.

Iyer-Pascuzzi, A. S., Symonova, O., Mileyko, Y., Hao, Y., Belcher, H., Harer, J., . . . Benfey, P. N. (2010). Imaging and analysis platform for automatic phenotyping and trait ranking of plant root systems. *Plant Physiol, 152*(3), 1148-1157. Retrieved from https://www.ncbi.nlm.nih.gov/pubmed/20107024. doi:10.1104/pp.109.150748

Ke, Lin, Liang, Gong, Yixiang, Huang, . . . Pan. Deep Learning-Based Segmentation and Quantification of Cucumber Powdery Mildew Using Convolutional Neural Network. *Frontiers in Plant Science*.

Kingma, D. P., & Ba, J. J. C. S. (2014). Adam: A Method for Stochastic Optimization.

Koller, T. M., Gerig, G., Szekely, G., & Dettwiler, D. (1995). *Multiscale detection of curvilinear structures in 2-D and 3-D imagedata.* Paper presented at the International Conference on Computer Vision.

Lin, T. Y., Goyal, P., Girshick, R., He, K., Dollar, P. J. I. T. o. P. A., & Intelligence, M. (2017). Focal Loss for Dense Object Detection. *PP*(99), 2999-3007.

Long, J., Shelhamer, E., & Darrell, T. (2015). *Fully convolutional networks for semantic segmentation.* Paper presented at the Proceedings of the IEEE conference on computer vision and pattern recognition.

Milletari, F., Navab, N., & Ahmadi, S. A. (2016). *V-Net: Fully Convolutional Neural Networks for Volumetric Medical Image Segmentation.* Paper presented at the Fourth International Conference on 3d Vision.

Pound, M. P., Atkinson, J. A., Townsend, A. J., Wilson, M. H., Griffiths, M., Jackson, A. S., . . . French, A. P. (2017). Deep machine learning provides state-of-the-art performance in image-based plant phenotyping. *Gigascience, 6*(10), 1-10. Retrieved from https://www.ncbi.nlm.nih.gov/pubmed/29020747. doi:10.1093/gigascience/gix083

Rebouillat, J., Dievart, A., Verdeil, J. L., Escoute, J., Giese, G., Breitler, J. C., . . . Périn, C. J. R. (2009). Molecular Genetics of Rice Root Development. *2*(1), 15-34.

Ronneberger, O., Fischer, P., & Brox, T. (2015). *U-Net: Convolutional Networks for Biomedical Image Segmentation.* Paper presented at the International Conference on Medical Image Computing & Computer-assisted Intervention.

Sekulska-Nalewajko, J., & Goclawski, J. (2009). *Segmentation and geometry identification of white roots in two-dimensional scanner images.* Paper presented at the International Conference on Perspective Technologies and Methods in Mems Design, 2009. Memstech.

Srivastava, N., Hinton, G., Krizhevsky, A., Sutskever, I., & Salakhutdinov, R. J. J. o. M. L. R. (2014). Dropout: a simple way to prevent neural networks from overfitting. *15*(1), 1929-1958.

Strack, D. J. P. (2001). Root Methods: A Handbook : Edited By A. L. Smit, A. G. Bengough, C. Engels, M. van Noordwijk, S. Pellerin and S. C. van de Geijn, Springer Press, Berlin Heidelberg, 2000, 587 pp. 108 figs., DM 198. ISBN 3-540-66728-8. *57*(1), 143-143.

Tracy, S., Black, C., Roberts, J., & Mooney, S. (2010). *Visualising the effect of compaction on root architecture in soil using X-ray Computed Tomography.* Paper presented at the 19th World Congress of Soil Science, Soil Solutions for a Changing World.

Yao, Z., Zhang, Z., & Xu, L. Q. (2016). *Convolutional Neural Network for Retinal Blood Vessel Segmentation.* Paper presented at the International Symposium on Computational Intelligence & Design.

Zhou, J., & Troyanskaya, O. G. (2015). Predicting effects of noncoding variants with deep learning-based sequence model. *Nat Methods, 12*(10), 931-934. Retrieved from https://www.ncbi.nlm.nih.gov/pubmed/26301843. doi:10.1038/nmeth.3547

Zobel, R. W., Kinraide, T. B., Baligar, V. C. J. P., & Soil. (2007). Fine root diameters can change in response to changes in nutrient concentrations. *297*(1/2), 243-254.

344

Table 1. Comparison between the different methods

Root	Method	Hausdorff Distance	DSC	IoU
	Otsu	408.2	0.655	0.487
1	U-net	282.7	0.916	0.845
	SE-ResUnet	283.0	0.936	0.880
	Otsu	307.6	0.643	0.473
2	U-net	282.7	0.915	0.844
	SE-ResUnet	283.0	0.937	0.882
	Otsu	411.6	0.662	0.495
3	U-net	89.0	0.916	0.846
	SE-ResUnet	88.2	0.936	0.880
	Otsu	154.3	0.743	0.591
4	U-net	77.3	0.898	0.815
	SE-ResUnet	77.3	0.921	0.854

345

346

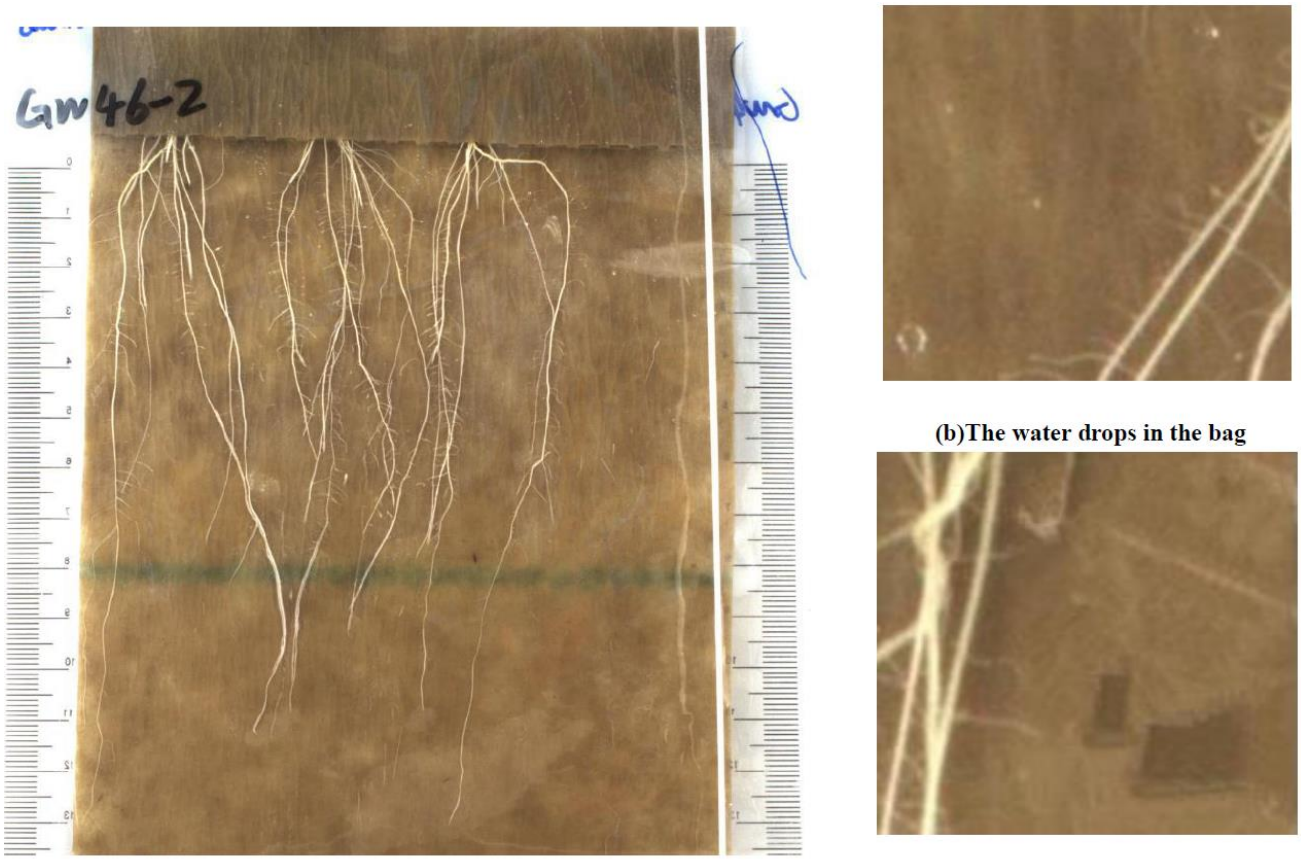

(a) Cultivation of the rice seedlings by transparent bag

(b)The water drops in the bag

(c) The reflective light

Figure 1. Captured root system of rice seedlings. The root is in its primitive shape and it clings to the capillary paper

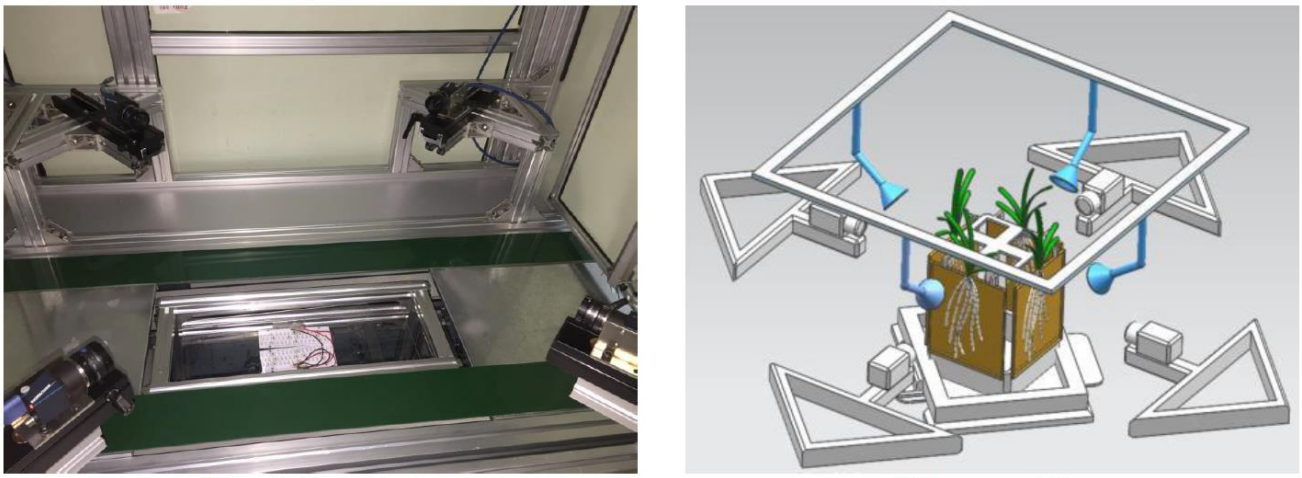

(a)Automatic imaging darkroom

(b) Image acquisition

Figure 2. The equipment for collect root image

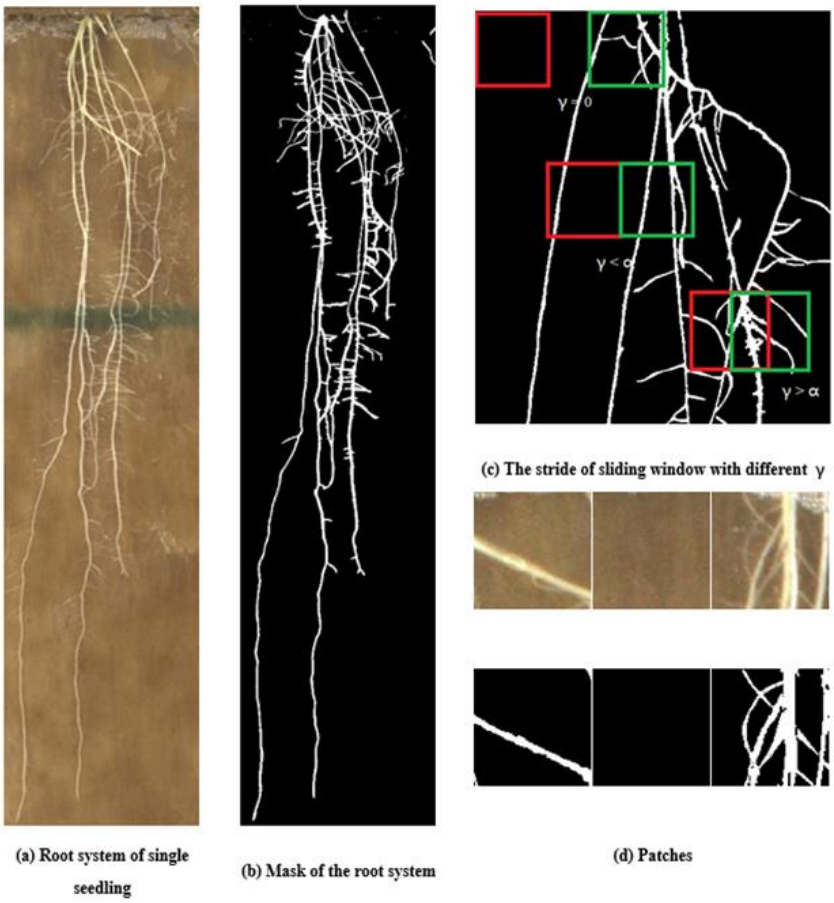

353
354 **Figure 3. Process the root images for CNN training**

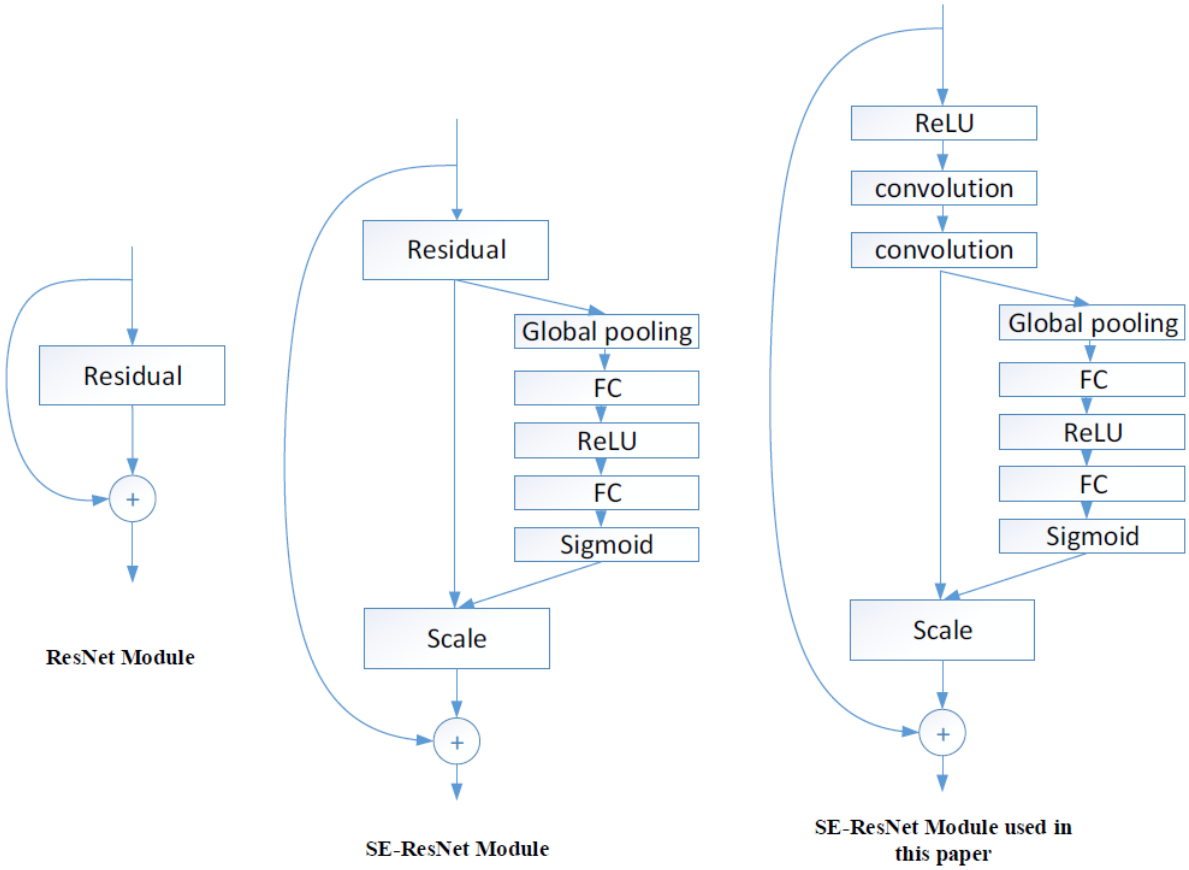

Figure 4. The residual module and SE-ResNet module. The residual is scaled by the small branch net. FC means the full connection layer

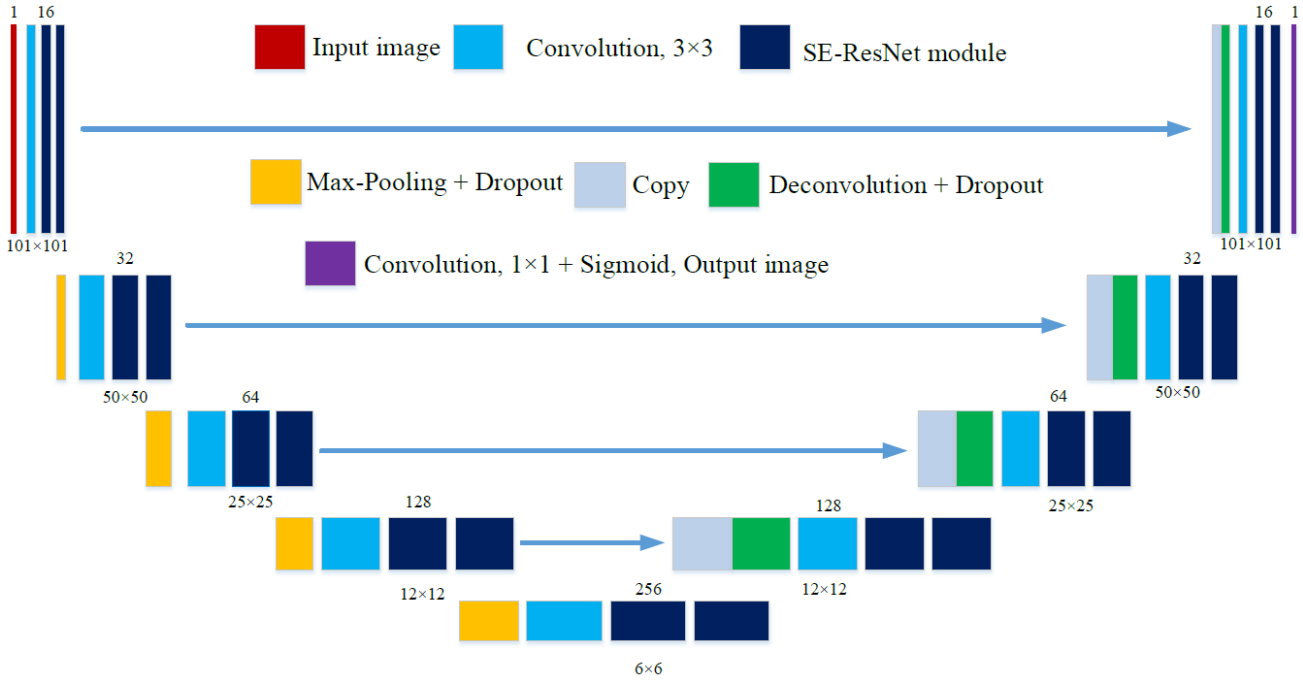

Figure 5. The structure of our SE-ResUnet

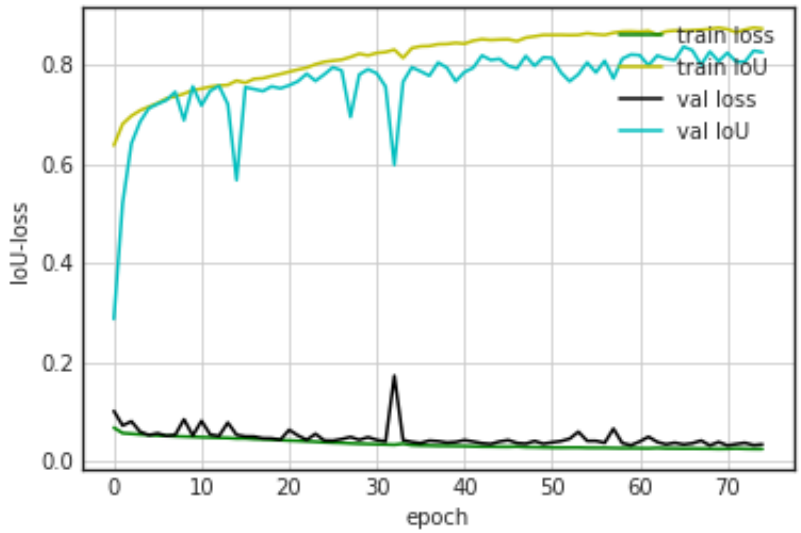

Figure 6. The convergence process on train set and validation set

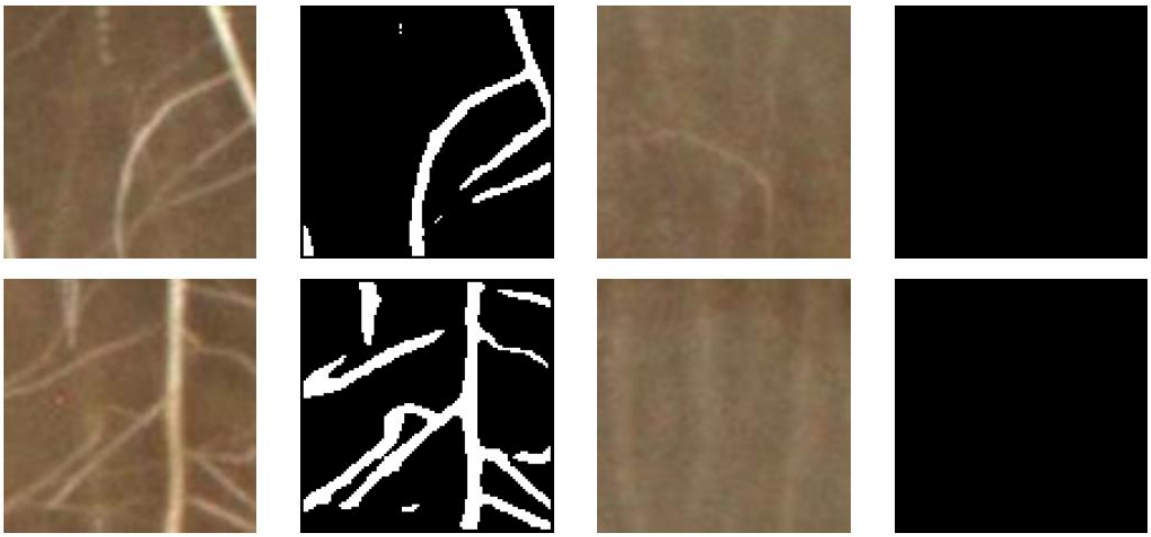

(a) The lateral root was well segmented **(b) The root-like noise was romoved**

Figure 7. The segmentation experiment of proposed model

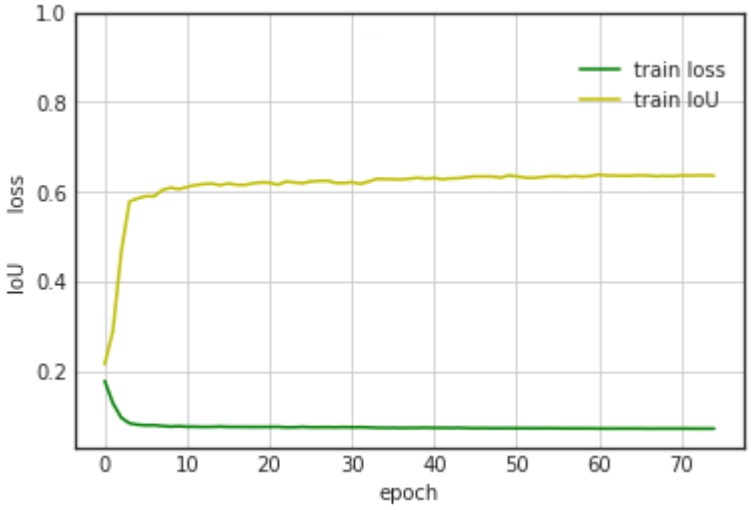

Figure 8. The convergence process of U-net

(a) Original root system image | (b) Segmentation result of Otsu | (b) Segmentation result of U-net | (d) Segmentation result of our model

Figure 9. The segmentation comparison between different methods

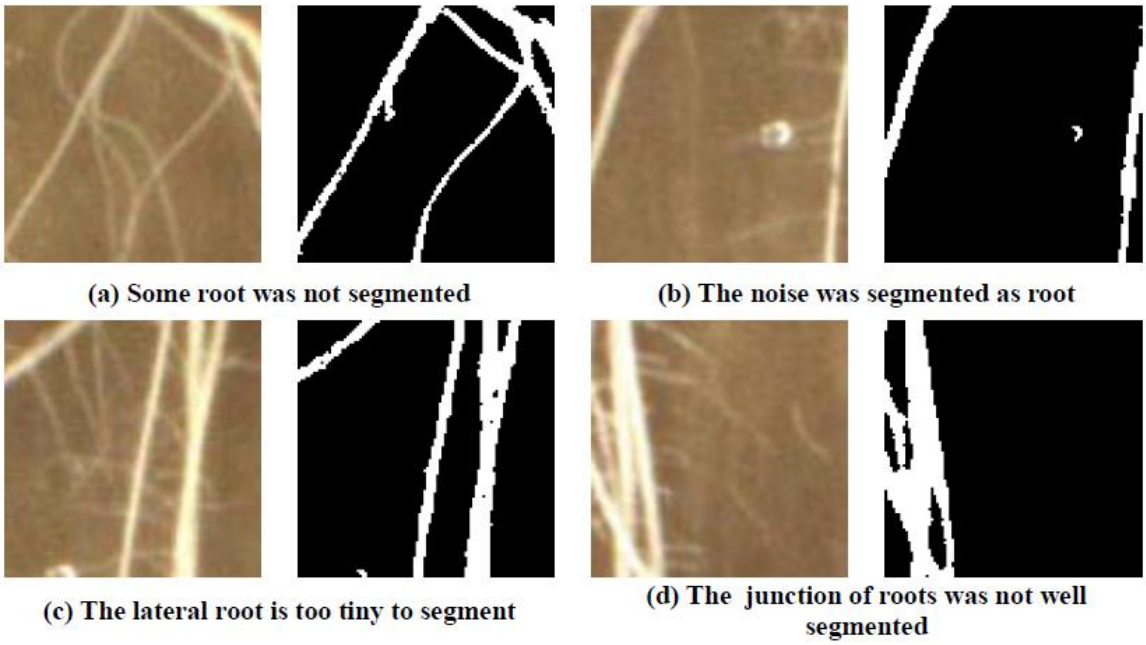

Figure 10.The defects of annotation image(mask)

Figure 11. The worst result